KLL Auger decay in free aluminum atoms

M. Huttula, L. Partanen, A. Mäkinen, T. Kantia, H. Aksela, and S. Aksela
Department of Physical Sciences, University of Oulu, P.O. Box 3000, 90014 Oulu, Finland
(Received 19 December 2008; published 9 February 2009)

The *KLL* Auger spectrum of atomic aluminum has been recorded applying electron impact for the creation of 1*s* core hole states. The experimental results are compared to predictions obtained with *ab initio* calculations for spectral structures.

DOI: 10.1103/PhysRevA.79.023412 PACS number(s): 32.80.Hd

I. INTRODUCTION

The *KLL* Auger transitions in free atoms present the simplest nonradiative electronic decay channel and therefore are of fundamental theoretical interest. Atomic spectra are advantageous for detailed theoretical analysis because the solid-state and molecular environments cause additional demands for the interpretation of spectra. Besides Ne [1,2] and Ar [3] rare gases, only the *KLL* spectra of Na [4] and Mg [5] atomic vapors were studied by Hillig *et al.* [4] and Breuckmann and Schmidt [5] in their pioneering works. Even for the commonly used x ray tube anode material aluminum the atomic spectrum for the 1*s* ionization and subsequent Auger decay does not exist. Therefore, it is very interesting to extend the *KLL* Auger studies to metallic elements having higher *Z*.

Experimental difficulties which have made these studies hard or impossible to carry out are the low 1*s* ionization cross section for electron impact, which decreases roughly inversely to the square of 1*s* binding energy, and the low vapor density of beam targets. Also rather high evaporation temperatures and high reactivity of liquid metals cause technical problems in vapor phase measurements generally. However, the data collection efficiency is increased by the position-sensitive detectors of modern electron spectrometers roughly by 2 orders of magnitude which has greatly promoted the studies of inherently low intensity transitions, such as the *KLL* Auger-electron emission of atomic Al.

Aluminum is one of the most commonly used materials in industry due to its physical properties such as good conductivity, light weight, inertness, durability, and pliability. Still for atomic aluminum, there exist only few previous electron spectroscopic studies on the *L* and *M* shells, which have the ionization cross sections essentially larger than the *K* shell. The electron-impact measurements of the autoionizing decay of the 3*s* states were studied by James *et al.* [6]. Dyke *et al.* [7] applied He I uv excitation to study outer valence photoelectron spectra (PES). Synchrotron radiation excited 2*p* PES and subsequent Auger-electron spectra (AES) of atomic aluminum were studied by Malutzki *et al.* [8]. Recently, the synchrotron radiation excited high-resolution spectra of *L* shell ionized atomic aluminum were reported with detailed interpretations for the 2*p* PES and the subsequent AES by Jänkälä *et al.* [9] and for the 2*s* PES and subsequent AES by Huttula *et al.* [10]. However, to our best knowledge, no experimental studies on *K* shell of atomic Al have been published whereas a variety of solid-state *KLL* AES experiments exists (see, e.g., [11,12]). Besides its basic structure, the *KLL* spectrum of atomic aluminum is considered to be interesting also as a reference for comparison to solid-state spectra in order to study different solid-state effects such as energy shifts, solid-state broadening, etc.

In the present work, a pulsed electron-impact excitation for the 1*s* core hole creation in atomic Al has been used. The electron impact is well suited for *KLL* experiments as cascade transitions following ionization of higher binding-energy orbitals do not exist. The inductively heated evaporation oven with synchronized pulsing of the electron beam and induction field [10] was used to produce Al vapor. The experimental results are compared to *ab initio* theoretical predictions obtained applying the Hartree-Fock (HF) method using Cowan's code [13].

II. EXPERIMENTS

The experiments were performed with a Gammadata-Scienta electron spectrometer based setup at the University of Oulu. The system consists of a home laboratory designed and manufactured vacuum chamber with multiple entrance ports to the interaction region, a 200 mm radius hemispherical electron energy analyzer with an *XYZ*-manipulator adjustable evaporation stage, a gas inlet system, and a liquid-nitrogen-cooled cold trap.

The Scienta SES-200 spectrometer equipped with position sensitive multichannel plate detector is updated with a high-resolution charge-coupled device (CCD) camera and SES-R4000 power supply unit. The Al vapor was generated in an inductively heated oven system described in [10]. Shortly, high-frequency alternating current is used to generate eddy currents in electrically conducting crucible providing heating due to resistive losses. The fluctuating magnetic and electric fields may interfere with primary electron beam as well as electrons emitted by the sample atoms. In order to record spectra, not affected by magnetic and electric field disturbances, heating process is pulsed. In the experimental system described in [14] and used in the high-temperature synchrotron radiation excited experiments on silicon [15], the electron signal from the Quantar multichannel plate (MCP) resistive anode detector is vetoed. In the present fluorescent screen based detection system, the vetoing is not readily possible due to the relative slow (15 frames per second) readout rate of the CCD camera and a compact software design of the Scienta electron analyzer. The problem has been overcome by synchronizing electron excitation to the heating se-

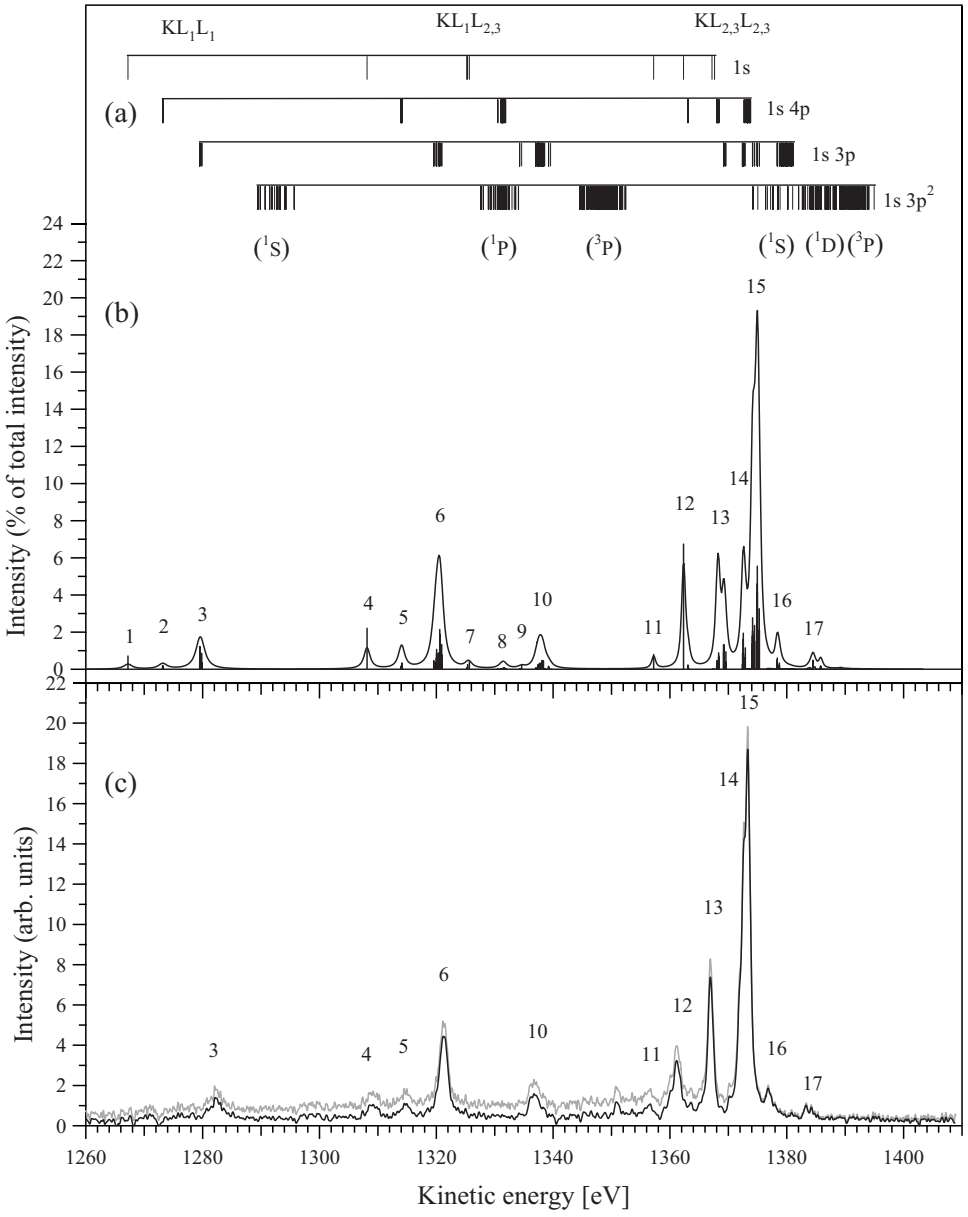

FIG. 1. *KLL* Auger spectrum of aluminum. (a) Calculated Auger energies (bars) are grouped according to initial configuration with connecting line. Parents of final-state terms are given below the bars. (b) Simulated *KLL* Auger spectra (envelope curve) and calculated Auger transitions (bars). Assignments for labels 1–17 are given in Table I. (c) Experimental spectrum measured using 4 keV electron impact with subtraction of Shirley background (black line) and linear background (gray line).

quence as follows. During the heating sequence, a synchronized pulse is provided for analogically controllable *XY* positioning of the impact electron beam to divert the beam away from the interaction region of the experiments. A special care is taken to ensure that the surface-scattered electrons of the impact beam at the "off position" are out of sight for the electron spectrometer. Thus, almost a zero count rate is obtained during heating period even while the electrons are recorded constantly.

Presently, we used 0.25 s sequences providing 0.09 s heating period with 5 kW power and 0.16 s measuring period. Thus only one third from the total time was lost in gating. Generally, the time period of sequences in high-temperature experiments is selected as short as possible in order to prevent variations in the crucible temperature. A short heating sequence also ensures that minor variations in experimental parameters are averaged to constant level during the scanning of kinetic-energy region over the position sensitive MCP detector. Additional averaging is obtained by producing the final spectrum as a sum of several single sweeps. However, the single sweep spectra were found to resemble closely each other within statistical variations.

The electron spectra of atomic Al were recorded at the 90° configuration relative to the propagation direction of the impact electron beam. The electron-impact energy of 4 keV was used to provide close to the maximum cross section for the Al 1*s* ionization. The primary electron current was around 150 μA measured with a Faraday cup behind the interaction region of experiment. A wolfram crucible was used with a boron nitride cap having a 10 mm long hole of 2 mm in diameter. The temperature inside the crucible was estimated to be around 1300 K. The partial pressure of Al vapor in effective source volume was only about 10^{-5} mbar, estimated with the aid of the Ne *KLL* Auger intensities which were measured simultaneously. The Al *KLL* AES presented in Fig. 1(c) was measured with a 100 eV pass energy using 0.8 mm curved entrance slit of the electron spectrometer resulting to approximately 280 meV analyzer contribution to

the linewidths. The transmission variations of the electron energy analyzer were expected to be negligible on the high kinetic energies of the *KLL* transitions. The kinetic energy of Al spectrum was calibrated by introducing Ne gas to the interaction region and recording the main Ne $KL_{2,3}L_{2,3}(^1D)$ Auger line at 804.456 eV kinetic energy [1] simultaneously with the *KLL* spectrum of Al. Inspection of experimental spectrum of Fig. 1(c) shows that the spectral background on the low energy side of the peaks is clearly higher. Therefore, the Shirley background, applied commonly to solid-state spectra, was reduced from the measured *KLL* spectrum using the algorithm in IGORPRO macro package [16]. Figure 1(c) shows both the Shirley background reduced spectra and the original data with linear background subtraction. It can be seen that the Shirley background works surprisingly well despite its artificiality to atomic spectra.

III. CALCULATIONS

The kinetic energies and transition rates of the *KLL* Auger transitions of aluminum were computed using Cowan's code [13]. The wave functions for the initial and final states were calculated in intermediate coupling scheme using the HF method with relativistic corrections (HFR) allowing the states having the same total angular momentum J and parity to mix by applying the configuration-interaction (CI) method. Spin-orbit interaction was calculated with the aid of the Blume-Watson theory [17]. The Slater integrals were not scaled. The HFR continuum orbitals were generated in the configuration-average potentials of each final electron configuration. The energies of continuum electrons were taken as difference between the configuration-average energies of initial and final electron configurations.

The primary core ionization can be accompanied also by the shake-up or shake-off transition of outer electron or the resonant excitation of a $1s$ electron most probably to the $3p$ unfilled orbital. In the calculations for single-ionized initial states, the $1s2s^22p^63s^23p$ and $1s2s^22p^63s^24p$ electron configurations were included. The corresponding final states were calculated for the doubly-ionized $1s^22s^02p^63s^2np$, $1s^22s2p^53s^2np$, and $1s^22s^22p^43s^2np$ ($n=3$ or 4) electron configurations. In addition, the Auger transitions from the resonantly excited states $1s^12s^22p^63s^23p^2$ to the $1s^22s^02p^63s^23p^2$, $1s^22s^12p^53s^23p^2$, and $1s^22s^22p^43s^23p^2$ states and from the $1s2s^22p^63s^2$ doubly-ionized initial states to the $1s^22s^02p^63s^2$, $1s^22s2p^53s^2$, and $1s^22s^22p^43s^2$ triply-ionized states were calculated.

The calculated *KLL* Auger energies and intensities are depicted in Fig. 1(b) with vertical bars together with a simulated Auger spectrum. For the simulated spectrum, the Auger line widths of 1.7, 1.2, and 0.7 eV for KL_1L_1, $KL_1L_{2,3}$, and $KL_{2,3}L_{2,3}$ Auger transitions, respectively, were obtained from the lifetime widths of the $1s$, $2s$, and $2p$ hole states of 0.7, 0.5, and 0.03 eV, respectively (for further details, see Sec. IV). The analyzer resolution of 0.28 eV was used as a Gaussian width in simulation. All the initial states within an initial configuration were assumed to be equally populated. The calculated intensities of the Auger transitions originating from the $1s2s^22p^63s^23p$, $1s2s^22p^63s^24p$, $1s2s^22p^63s^2$, and $1s^12s^22p^63s^23p^2$ initial states were scaled to correspond to the experimental intensity ratio. The results are discussed in Sec. IV.

IV. RESULTS AND DISCUSSION

The *KLL* Auger spectrum of neon is well known (see, e.g., [2] and references therein). The Ne *KLL* Auger spectrum consists of the $KL_1L_1(^1S_0)$, $KL_1L_{2,3}(^1P_1)$, and $(^3P_{0,1,2})$, and $KL_{2,3}L_{2,3}(^1S_0)$ and $(^1D_2)$ lines, while the $KL_{2,3}L_{2,3}(^3P)$ lines are not visible in the spectrum [2]. Additionally, the *KLL* Auger spectrum of Ne has a rich shake-up and shake-off satellite structures [2]. The ground state Al configuration has the $3s^23p$ configuration above the neon structure which leads to additional splitting of energy levels both in the initial and final states of the *KLL* Auger transition due to coupling between the core holes and the valence $3p$ electron. The initial state of the Al *KLL* normal Auger transitions is singly ionized. The *LS* coupling of the $1s$ hole and the valence $3p$ electron leads to four *LSJ* initial states, $^1P_1$ and $^3P_{0,1,2}$. For the satellite Auger structure, the term symbols of the $1s^{-1}4p$ shake-up states are the same as for the initial states of the normal Auger transitions. Additionally, there are eight resonantly excited $1s^{-1}3p^2$ initial states of which five are doublet states, and the $1s^{-1}3p^{-1}\ ^2S_{1/2}$ doubly-ionized initial state. For the Al^{2+} final states, coupling between the $(2s,2p)^{-2}$ core holes produces the same parent terms as for the neon final states, which are further coupled with the valence $3p$ electron (or electrons), which leads to 41 doubly-ionized final states of the normal *KLL* Auger transitions.

The calculated *KLL* and satellite Auger transition energies of Al are depicted in Fig. 1(a) with vertical bars. The KL_1L_1, $KL_1L_{2,3}$, and $KL_{2,3}L_{2,3}$ Auger groups are labeled above bars. The open shells in the initial-state configuration are given on the right side of bars. Occupation of the outer $3s$ and $3p$ orbitals is assumed not to change during the Auger decay. In Fig. 1(a), the *LSJ* terms below bars are the parent terms of the final states originating from the $(2s,2p)^{-2}$ configuration. The valence p electron does not split the parent state much as the final states having the same parent state are located very close to each other. Consequently, different states inside a parent core hole state cannot be separated from each other in the experimental spectrum because of the large natural widths of the *KLL* Auger lines.

Figure 1(b) shows the simulated *KLL* Auger and satellite spectrum of aluminum, which agrees very well with the experimental spectrum measured with electron impact in the *KLL* Auger region and shown in Fig. 1(c). The triple peak structure at the kinetic-energy region 1260–1290 eV labeled as 1–3 originates from the KL_1L_1 Auger transitions. The main Auger transitions from the $1s^12s^22p^63s^23p$ initial states at the kinetic energy of about 1282 eV are the most intense KL_1L_1 peaks. The satellite Auger transitions for the KL_1L_1 structure from the $1s^12s^22p^63s^24p$ shake-up and $1s^12s^22p^63s^2$ shake-off initial states are located at about 7 and 12 eV lower kinetic energies, respectively, but they are hardly observable in the experimental spectrum. The $KL_1L_{2,3}$

TABLE I. Experimental kinetic energies (KE) and relative intensities of Al *KLL* Auger peaks. Peak labels refer to Fig. 1. *LS*-coupled initial and final states are obtained with the aid of HF calculations. The fully occupied orbitals of the initial and final configurations has not been written in columns 4 and 5.

Peak	KE (eV)	Int. (%)	Initial state	Final state
1	1270.50	0.48	$Al^{2+}1s$	$Al^{3+}2s^02p^6(^1S_0)$
2	1276.49	1.02	$Al^{+}1s4p$	$Al^{2+}2s^02p^64p(^2P_{1/2,3/2})$
3	1282.40	4.89	$Al^{+}1s3p$	$Al^{2+}2s^02p^63p(^2P_{1/2,3/2})$
4	1309.08	1.92	$Al^{2+}1s$	$Al^{3+}2s2p^5(^1P_1)$
5	1314.77	1.88	$Al^{+}1s4p$	$Al^{2+}2s2p^5(^1P)4p(^2P,\ ^2D)$
6	1321.21	11.86	$Al^{+}1s3p$	$Al^{2+}2s2p^5(^1P)3p(^2S,\ ^2P,\ ^2D)$
7	1324.95	0.74	$Al^{2+}1s$	$Al^{3+}2s2p^5(^3P_2)$
8	1330.34	0.52	$Al^{+}1s4p$	$Al^{2+}2s2p^5(^3P)4p$
9	1334.25	0.35	$Al^{+}1s3p$	$Al^{2+}2s2p^5(^3P)3p(^2S_{1/2})$
10	1337.00	4.37	$Al^{+}1s3p$	$Al^{2+}2s2p^5(^3P)3p$
	1350.95	1.70		
11	1356.40	1.46	$Al^{2+}1s$	$Al^{3+}2s^22p^4(^1S_0)$
12	1361.09	7.94	$Al^{2+}1s$	$Al^{3+}2s^22p^4(^1D_2)$
13	1366.93	12.17	$Al^{+}1s4p$ / $Al^{+}1s3p$	$Al^{2+}2s^22p^4(^1D)4p(^2P,\ ^2D,\ ^2F)$
14	1372.47	17.70	$Al^{+}1s3p$	$Al^{2+}2s^22p^4(^1D)3p(^2P)$
15	1373.36	27.69	$Al^{+}1s3p$	$Al^{2+}2s^22p^4(^1D)3p(^2D,\ ^2F)$
16	1376.96	2.20	$Al^{+}1s3p$	$Al^{2+}2s^22p^4(^3P)3p(^2P)$ [a]
17	1383.40	1.11	$Al\ 1s^13p^2$	$Al^{+}2s^22p^43p^2$
		$\Sigma=100.00$		

[a]Forbidden in *LS* coupling; states are mixing with $2s^22p^4(^3P)3p(^2D)$.

and $KL_{2,3}L_{2,3}$ Auger groups are located at the kinetic-energy regions 1306–1340 and 1353–1388 eV, respectively. The energy splittings of 7 and 12 eV between the main and shake-up and shake-off satellite structures are found also in the $KL_1L_{2,3}$ and $KL_{2,3}L_{2,3}$ groups. The $KL_1L_{2,3}$ Auger group shows four well-resolved peaks, 4–6 and 10, and two very weak peaks, 7 and 8. The $KL_{2,3}L_{2,3}$ Auger spectrum consists of seven peaks, 11–17, of which the peaks 14 and 15 are merged. The resonant Auger transitions produce only the peak 17 while other resonant Auger transitions are too weak to be resolved.

The peaks labeled as 1–17 in the experimental Auger spectrum in Fig. 1(c) can be assigned with the aid of the simulated Auger spectrum in Fig. 1(b). The initial and final states of Auger transitions are given in Table I with experimental Auger energies and intensities. The $1s2s^22p^63s^2np$ $^1P_1$ and $^3P_{0,1,2}$ initial states ($n=3,4$) give an equal contribution to Auger transitions, so only the initial configurations are given in Table I. For final states, dominant *LS*-coupled terms with a parent term are given. The most intense *KLL* Auger transitions are the $1s2s^22p^63s^23p \rightarrow 1s^22s^22p^4(^1D)3s^23p$ transitions between the $^3P_2 \rightarrow {}^2F_{7/2}$, $^3P_0 \rightarrow {}^2F_{5/2}$, and $^3P_1 \rightarrow {}^2F_{5/2}$ states with calculated relative intensities of 4.5%, 5.5%, and 4.1%, respectively, which are located at 1373.4 eV (peak 15). A double structure of peak 15 is seen both in experimental and simulated spectra. The lower peak originates from transitions to the $1s^22s^22p^4(^1D)3s^23p\ ^2D_J$ states and the higher peak from transitions to the $1s^22s^22p^4(^1D)3s^23p\ ^2F_J$ states. The most intense $KL_1L_{2,3}$ Auger transitions are located at the kinetic energy of 1321.2 eV (peak 6) and they are assigned to originate from the $1s2s^22p^63s^23p \rightarrow 1s^22s2p^5(^1P)3s^23p$ transitions between the $^3P_2 \rightarrow {}^2D_{5/2}$, $^3P_0 \rightarrow {}^2D_{3/2}$, and $^3P_1 \rightarrow {}^2D_{3/2}$ states.

The $KL_{2,3}L_{2,3}$ Auger transitions to ^3P parent states are forbidden in *LS* coupling without a violation of the selection rule $\Delta L=0$. Therefore, these Auger transitions are expected to be very weak. However, peak 16 is assigned to originate from these forbidden transitions with relative intensity of 2.2% of the total intensity of the experimental *KLL* spectrum. The explanation for even this high intensity is found in a strong mixing with the final $1s^22s^22p^4(^1D)3s^23p\ ^2P$ and $1s^22s^22p^4(^3P)3s^23p\ ^2P$, $J=1/2$, 3/2 states. The mixing between the states having the same total angular-momentum quantum number J arises via spin-orbit interaction, and calculations predicted these final states to gain 2.3% of the total intensity of the *KLL* transitions. The same kind of behavior was found in the theoretical study for the $KL_{2,3}L_{2,3}$ Auger transitions of the $3s \rightarrow 3p$ laser-excited sodium [18]. Also the Auger transitions from the initial singlet $^1P_1$ state to quartet states are forbidden in *LS* coupling (selection rule $\Delta S=0$) but, however, weak transition probabilities were predicted

due to the intermediate coupling. Generally, very low transition rates to quartet states were predicted for all initial states, transition rates being about 4% of the total transition rate.

The intensity ratio between the KL_1L_1 (peaks 1–3), $KL_1L_{2,3}$ (peaks 4–10), and $KL_{2,3}L_{2,3}$ (peaks 11–16) Auger groups was determined in this work, and the experimental intensity ratio was found to be 6%, 23%, and 71%, respectively. Calculations reproduce this intensity ratio fairly well being 8%, 23%, and 69%. The KL_1L_1 group rate is slightly overestimated by calculations at the expense of the $KL_{2,3}L_{2,3}$ group rate. CI transfers some transition rate from the $1s^22s^02p^63s^2np$ ($n=3,4$, or ε) final states to the $1s^22s^22p^43s^2np$ ($n=3,4$, or ε) final states. The intensity ratios between the main *KLL* ($np=3p$), shake-up *KLL* ($np=4p$), and shake-off *KLL* ($np=\varepsilon l$) Auger groups were determined from experiments to be about 77%, 12%, and 11%, respectively.

The calculated total decay rate for each initial $^1P_1$ and ^3P_J is $\Gamma=1.380\times10^{-2}$ a.u. (0.38 eV), which is much smaller than the $1s^{-1}$ state lifetime width of 0.7 eV, which is the width of the x-ray $K\alpha$ radiation commonly used in x-ray physics [19]. The lifetime width of initial state equals to the natural width of Auger lines if the final states cannot further decay via Auger transition. Instead, if the Auger final state continues decaying by a subsequent Auger transition, the natural width of the first step Auger transitions is a convolution of the lifetime widths of initial and final states. The $2s$ and $2p$ Auger spectra were measured and studied previously in [9,10]. The $2s^{-1}$ states were found to decay to the $2p^{-1}(3s3p)^{-1}$ states via fast Coster-Kronig transitions, and the natural linewidths of the $2s$ ionized states were found to be 0.5 eV [10]. The $2p^{-1}$ states decay via $L_{2,3}MM$ Auger transitions, and the natural width of $2p$ is very narrow—about 0.03 eV. Thus the natural width of the $KL_{2,3}L_{2,3}$ Auger transitions is close to the initial-state lifetime width. The KL_1L_1 and $KL_1L_{2,3}$ Auger transitions have broader line widths than the lifetime width of the $1s^{-1}$ initial state, which is due to the fact that $2s^{-2}$ and $2s^{-1}2p^{-1}$ vacancies are filled during the subsequent Coster-Kronig and Auger transitions by $2p$, $3s$, and $3p$ electrons. The kinetic energy of the main $KL_{2,3}L_{2,3}$ Auger peak (weighted average of peaks 14 and 15) at 1373.0 eV can be compared to corresponding solid-state values of 1393.3 eV [20], 1393.4 eV [12], and 1393.55 eV [21]. By taking the work function of 4.2 eV into account, the solid-state Auger energy shift of about 16.0 eV is obtained.

V. CONCLUSIONS

The *KLL* Auger spectrum of atomic aluminum was measured using electron impact for creation of a $1s$ core hole. The high-resolution and high-sensitive electron spectrometer setups at the University of Oulu with sequenced induction heating were used to record the spectrum. The *KLL* Auger spectrum was predicted using the Hartree-Fock wave functions for the $1s$ ionized initial states and $(2s,2p)^{-2}$ final states both for the main and satellite electron configurations. The Al *KLL* Auger spectrum of good quality was interpreted with the aid of calculations. The intensity ratios of 2%, 23%, and 75% between the KL_1L_1, $KL_1L_{2,3}$, and $KL_{2,3}L_{2,3}$ Auger groups, respectively, were obtained. The intensity ratio between the main and satellite Auger transitions was obtained to be distributed between the main, $3p\rightarrow4p$ shake-up, and shake-off *KLL* Auger groups as about 77%, 12%, and 11%. Electron correlation was found to play a negligible role in the *KLL* transitions.

ACKNOWLEDGMENTS

P. Kovala is acknowledged for assistance during the measurements. This work has been financially supported by the Research Council for Natural Sciences and Technology of the Academy of Finland and Yrjö, Urho ja Kalle Väisälä foundation.

[1] H. Körber and W. Mehlhorn, Phys. Lett. **13**, 129 (1964); H. Körber and W. Mehlhorn, Z. Phys. **191**, 217 (1966).
[2] M. Leväsalmi, H. Aksela, and S. Aksela, Phys. Scr., T **41**, 119 (1992).
[3] M. Krause, Phys. Rev. Lett. **34**, 633 (1975); L. Asplund, P. Kelfre, B. Blomster, H. Siegbahn, and K. Siegbahn, Phys. Scr. **16**, 268 (1977).
[4] H. Hillig, B. Cleff, W. Mehlhorn, and W. Schmitz, Z. Phys. **268**, 225 (1974).
[5] B. Breuckmann and V. Schmidt, Z. Phys. **268**, 235 (1974).
[6] G. K. James, L. F. Forrest, K. J. Ross, and M. Wilson, J. Phys. B **18**, 775 (1985).
[7] J. M. Dyke, M. Feher, M. P. Hastings, A. Morris, and A. J. Paul, Mol. Phys. **58**, 161 (1986).
[8] R. Malutzki, A. Wachter, V. Schmidt, and J. E. Hansen, J. Phys. B **20**, 5411 (1987).
[9] K. Jänkälä, S. Fritzsche, M. Huttula, J. Schulz, S. Urpelainen, S. Heinäsmäki, S. Aksela, and H. Aksela, J. Phys. B **40**, 3435 (2007).
[10] M. Huttula, K. Jänkälä, A. Mäkinen, H. Aksela, and S. Aksela, New J. Phys. **10**, 013009 (2008).
[11] G. Dufour, J.-M. Mariot, P.-E. Nilsson-Jatko, and R. C. Karnatak, Phys. Scr. **13**, 370 (1976).
[12] B. Timmermans, N. Vaeck, A. Hubin, and F. Reniers, Surf. Interface Anal. **34**, 356 (2002).
[13] R. D. Cowan, *The Theory of Atomic Structure and Spectra* (University of California, Berkeley, 1981).
[14] M. Huttula, S. Heinäsmäki, H. Aksela, E. Kukk, and S. Aksela, J. Electron Spectrosc. Relat. Phenom. **156-158**, 270 (2007).
[15] K. Jänkälä, S. Urpelainen, M. Huttula, S. Fritzsche, S. Heinäsmäki, S. Aksela, and H. Aksela, Phys. Rev. A **77**, 062504 (2008).
[16] http://www.geocities.com/ekukk/
[17] M. Blume and R. E. Watson, Proc. R. Soc. London, Ser. A **270**, 127 (1962); **271**, 565 (1963).
[18] B. Lohmann, S. Fritzsche, and F. P. Larkins, J. Phys. B **29**,

3799 (1996).

[19] K. Siegbahn, C. Nordling, A. Fahlman, R. Nordberg, K. Hamrin, J. Hedman, G. Johansson, T. Bergmark, S.-E. Karlsson, I. Lindgren, and B. Lindberg, *ESCA—Atomic, Molecular and Solid State Structure Studied by Means of Electron Spectroscopy*, Nova Acta Regiae Societatis Scientiarum Upsaliensis Series IV, Vol. 20 (Almqvist & Wiksells Boktryckeri AB, Uppsala, 1967).

[20] J. A. Taylor, J. Vac. Sci. Technol. **20**, 751 (1982).

[21] L. P. H. Jeurgens, W. G. Sloof, F. D. Tichelaar, and E. J. Mittemeijer, Surf. Sci. **506**, 313 (2002).